Volume 23
Number 33
7 September 2021
Pages 17737–18228

PCCP

Physical Chemistry Chemical Physics

rsc.li/pccp

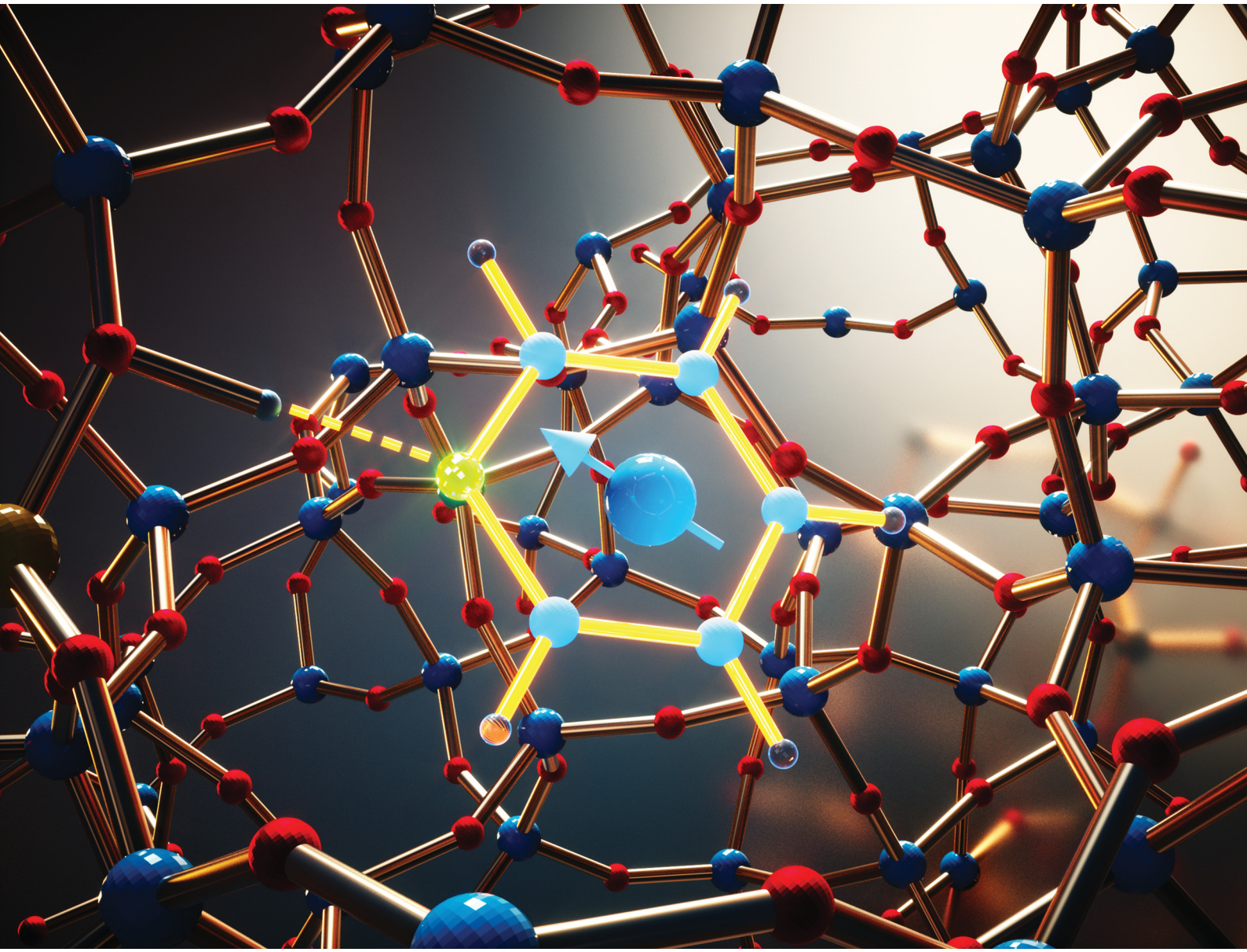

ISSN 1463-9076

ROYAL SOCIETY OF CHEMISTRY

PAPER

Carmine D'Agostino *et al.*

Nuclear spin relaxation as a probe of zeolite acidity: a combined NMR and TPD investigation of pyridine in HZSM-5

PCCP

PAPER

View Article Online
View Journal | View Issue

Open Access Article. Published on 18 June 2021. Downloaded on 10/16/2025 2:56:31 PM.
This article is licensed under a Creative Commons Attribution 3.0 Unported Licence.

Check for updates

Cite this: *Phys. Chem. Chem. Phys.*, 2021, **23**, 17752

Nuclear spin relaxation as a probe of zeolite acidity: a combined NMR and TPD investigation of pyridine in HZSM-5†

Neil Robinson,[a] Pierre Bräuer,[b] Andrew P. E. York[c] and Carmine D'Agostino *[d]

Received 7th April 2021,
Accepted 17th June 2021

DOI: 10.1039/d1cp01515j

rsc.li/pccp

The relative surface affinities of pyridine within microporous HZSM-5 zeolites are explored using two-dimensional ^{1}H nuclear magnetic resonance (NMR) relaxation time measurements. The dimensionless ratio of longitudinal-to-transverse nuclear spin relaxation times T_1/T_2 is shown to exhibit strong sensitivity to the silica/alumina ratio (SAR) of these zeolites, which is indicative of material acidity. This trend is interpreted in terms of increased pyridine surface affinity with decreasing SAR. Temperature programmed desorption (TPD) analysis corroborates this observation, revealing a distinct increase in the heat of desorption associated with adsorbed pyridine as a function of decreasing SAR. A direct correlation between NMR and TPD data suggests NMR relaxation time analysis can be a valuable tool for the non-invasive characterisation of adsorption phenomena in microporous solids.

Introduction

Microporous solids (exhibiting pore diameters <2 nm) such as zeolites and metal organic frameworks have potential applications across a variety of processes including chemical conversion, storage, sensing and separations.[1,2] In the field of heterogeneous catalysis zeolites are regularly applied to facilitate a range of reactions such as cracking,[3,4] alkylation[5] and dehydration.[6–8] A key feature regarding the activity of such materials is that of surface acidity, characterised by the presence of Brønsted (proton donating) and/or Lewis (electron accepting) acid sites within the micropore network, and across the external material surface. As both the accessibility and acidity of these sites dictate the potential catalytic activity of zeolitic materials, extensive research efforts have been directed towards their characterisation.[9,10]

Established techniques used to investigate the surface acidity of zeolites include infrared (IR) spectroscopy, temperature programmed desorption (TPD) and nuclear magnetic resonance (NMR) spectroscopy. The use of IR spectroscopy with pyridine as a probe molecule, for example, is particularly powerful since the assignment of vibrational modes associated with pyridinium ions at Brønsted sites and the coordination of complexes at Lewis sites are well-established.[11–13] Quantitative analysis in terms of adsorbate density is also possible if molar extinction coefficient values are known.[14] TPD analysis – again utilising basic probe molecules such as ammonia and pyridine – is also widely applied.[15–19] Typical TPD spectra report the desorption rate of the chosen probe molecule as a function of temperature; the area beneath such a curve is proportional to the amount of adsorbate present, providing quantification of acid site density, while the position of desorption peaks provides information on acid site strength. Magic angle spinning (MAS) solid state NMR spectroscopy measurements of zeolitic materials are extensively reported; such measurements provide a direct and quantitative probe of Brønsted acid site density *via* ^{1}H (proton) analysis and utilise the observed ^{1}H chemical shift values to both characterise site acidity[20] and differentiate between bridging (Si–OH–Al) and terminal (Al–OH or Si–OH) groups.[21] The measurement of ^{29}Si and ^{27}Al spectra also allows quantification of the material silica/alumina ratio (SiO_2/Al_2O_3), which is considered an analogue of zeolite acidity.[22] Indirect measurements of acid site characteristics are again possible *via* the use of probe molecules and facilitate the investigation of site accessibility. While ^{1}H chemical shift features may be exploited to detail probe molecule interactions, a wide range of heteronuclear MAS NMR experiments (including ^{13}C, ^{15}N and ^{31}P) have also been used to resolve adsorbate resonances.[23–27]

In the present work we detail an alternative magnetic resonance technique for the comparison and characterisation

[a] Department of Chemical Engineering, University of Western Australia, 35 Stirling Highway, Perth, WA 6009, Australia
[b] Department of Chemical Engineering and Biotechnology, University of Cambridge, Philippa Fawcett Drive, Cambridge, CB3 0AS, UK
[c] Johnson Matthey Technology Centre, Blount's Court, Sonning Common, Reading, RG4 9NH, UK
[d] Department of Chemical Engineering and Analytical Science, University of Manchester, The Mill, Sackville Street, Manchester, M13 9PL, UK. E-mail: carmine.dagostino@manchester.ac.uk

† Electronic supplementary information (ESI) available: Supplementary TPD discussion. See DOI: 10.1039/d1cp01515j

 This journal is © the Owner Societies 2021

Open Access Article. Published on 18 June 2021. Downloaded on 10/16/2025 2:56:31 PM.
This article is licensed under a Creative Commons Attribution 3.0 Unported Licence.

of zeolitic acidity based on analysis of the ^{1}H nuclear spin relaxation characteristics of a liquid-phase basic probe molecule. The past decade has seen a rapid evolution in the application and interpretation of nuclear spin relaxation phenomena as a probe of surface affinity and adsorbate behaviour within catalytically active porous media.[28,29] These measurements exploit relevant NMR pulse sequences to determine the rates longitudinal and/or transverse nuclear spin relaxation processes, which are characterised by the time constants T_1 and T_2, respectively. Within the unrestricted bulk liquid phase these time constants are known to conform to well-established relationships with molecular rotational and translational dynamics.[30] For liquids imbibed within porous solids, however, the correspondence between time constants and molecular dynamics is influenced by the pore structure and surface chemistry properties of the confining material, providing a potential route for the non-destructive characterisation of adsorption phenomena and confinement effects.

For fluids confined to catalytically active porous media the evaluation and interpretation of dimensionless relaxation time ratios is often of particular utility.[31,32] The ratio of longitudinal-to-transverse nuclear spin relaxation time constants T_1/T_2 is now established as a non-invasive probe of surface affinity,[33] and is a regularly sought metric to aid in the evaluation mesoporous catalyst materials.[34–38] Most notably, this ratio has been shown to correlate with the desorption energetics of liquids imbibed within mesoporous oxide materials as evaluated *via* both experimental[32] (TPD) and theoretical[39] (density functional theory) methods, and has been demonstrated as a useful probe of competitive adsorption processes in liquid-phase catalytic systems.[40–42] It is of interest to note, however, that this approach is yet to be applied to the evaluation of liquid-saturated microporous materials, with previous relaxation studies instead focussing on the investigation of gas admission and storage phenomena,[43–46] surface area screening protocols[47,48] and the study of confinement effects.[49–52] To this end, we detail here the measurement and interpretation of T_1/T_2 ratios exhibited by pyridine confined to the microporous zeolite HZSM-5 with varying silica/alumina ratios (SAR, a measure of zeolite acidity). Through a direct comparison with TPD analysis our results demonstrate for the first time a clear correlation between nuclear spin relaxation characteristics, SAR and pyridine desorption energetics.

Relaxation theory

For fluids confined to porous media the observed rates of nuclear spin relaxation T_i^{-1} (with $i \in \{1,2\}$) may be expressed as a linear combination of unrestricted bulk, surface, and topological contributions,[53]

$$\frac{1}{T_i} \approx \frac{1}{T_{i,\text{bulk}}} + \frac{2\alpha\rho_i}{d_p}\left(1 + \frac{\rho_i d_p}{4D}\right)^{-1} \approx \underbrace{\frac{1}{T_{i,\text{bulk}}}}_{\text{unrestricted}} + \underbrace{\frac{2\alpha\rho_i}{d_p}}_{\text{surface}} + \underbrace{\frac{8\alpha D}{d_p^2}}_{\text{topology}}. \quad (1)$$

Additional terms may also be required to fully describe transverse relaxation (i = 2) rates due to the influence of magnetic susceptibility differences between the confining solid and imbibed fluid.[54,55] Here $T_{i,\text{bulk}}^{-1}$ and D are the relaxation rates and self-diffusion coefficient of the unrestricted bulk fluid, respectively, α is a shape parameter that takes values of 1, 2 or 3 for planar, cylindrical or spherical pores, respectively, and d_p is the pore diameter. The surface relativities $\rho_i = \delta T_{i,\text{surf}}^{-1}$ are defined by the relaxation rates of species at the pore surface $T_{i,\text{surf}}^{-1}$ weighted by the length-scale of the adsorbed surface layer δ.[56] Enhanced rates of relaxation occur at the solid–liquid interface due to the reduction in rotational and translational molecular mobility upon adsorption[35,57] and through interactions with any paramagnetic species imbedded within the solid matrix,[58,59] such that $T_{i,\text{surf}}^{-1} \gg T_{i,\text{bulk}}^{-1}$. As $T_{i,\text{surf}}$ exhibits sensitivity to the surface chemistry of the porous medium under investigation,[60–62] this parameter is central to the characterisation of surface interactions using nuclear spin relaxation measurements.[63]

There exists two limiting cases for eqn (1), which may be defined according to the dimensionless parameter[59]

$$\kappa \equiv \frac{\rho_i d_p}{D}. \quad (2)$$

If $\kappa \gg 1$ a diffusion-limited condition arises, typically associated with large pores, slowly diffusing probe molecules and/or large surface relaxivities. In this case eqn (1) reduces to

$$\frac{1}{T_i} \approx \frac{1}{T_{i,\text{bulk}}} + \frac{8\alpha D}{d_p^2}, \quad (3)$$

such that the observed relaxation rates are dominated by the topology of the confining pore structures and the diffusive characteristics of the probe fluid.[59] Diffusion-limited relaxation has been observed for water confined between SiC grains exhibiting a high surface concentration of paramagnetic Fe^{3+} ions, resulting in large ρ_1 and ρ_2 values.[64] Sensitivity to the term d_p^{-2} means this regime is also of relevance to porous structures exhibiting small pore diameters on the same length scale as the probe molecules employed, as has been evidenced using calibrated microporous silica glasses.[51,52] Alternatively, if $\kappa \ll 1$ a surface-limited condition arises, associated with the presence of rapidly diffusing species and/or slow rates of surface relaxation. In this regime the rate of mixing between surface and bulk populations is rapid compared to the rates of surface relaxation and eqn (1) reduces to

$$\frac{1}{T_i} \approx \frac{1}{T_{i,\text{bulk}}} + \frac{2\alpha\rho_i}{d_p}, \quad (4)$$

such that the observed rates of relaxation exhibit sensitivity to the surface relaxivities ρ_i. Furthermore, as the regularly applied assumption of spherical pores (α = 3) gives‡

$$\frac{1}{T_i} \approx \frac{1}{T_{i,\text{bulk}}} + \rho_i \frac{S}{V}, \quad (5)$$

where S/V is the surface-to-volume ratio of the confining pore structure, ρ_i is often considered a scaling parameter between observed relaxation characteristics and pore size.[65,66]

‡ Here we recall that the surface-to-volume ratio (S/V) of a sphere of diameter d_{sphere} may be expressed as $S/V = 6/d_{\text{sphere}}$.

Open Access Article. Published on 18 June 2021. Downloaded on 10/16/2025 2:56:31 PM. This article is licensed under a Creative Commons Attribution 3.0 Unported Licence.

In the case of microporous zeolites careful consideration of an appropriate form of such expressions is required. In the present case, that of pyridine relaxation within HZSM-5 with various SAR, we note that the micropore diameter (d_p = 5.1–5.6 Å)[67] and molecular kinetic diameter ($d_k \approx$ 5.3 Å)[68] are essentially identical, such that there will be no contribution to the observed relaxation rates from bulk liquid away from the pore walls. An appropriate relaxation expression is therefore

$$\frac{1}{T_i} \approx \frac{2\alpha\rho_i}{d_p} + \frac{8\alpha D}{d_p^2}, \tag{6}$$

comprising only the surface and topological terms of eqn (1). A value of $\alpha = 2$ is suggested as a sensible shape parameter choice given the cylindrical pore structure exhibited by ZSM-5 zeolites,[69] such that this equation might be written

$$\frac{1}{T_i} \approx \frac{4}{d_p}\left(\rho_i + \frac{4D}{d_p}\right). \tag{7}$$

The corresponding ratio of observed relaxation time constants then becomes

$$\frac{T_1}{T_2} \approx \frac{\rho_2 + (4D/d_p)}{\rho_1 + (4D/d_p)}, \tag{8}$$

where the equivalence between d_k and d_p means the surface relaxivities may be expressed $\rho_i \approx d_k T_{i,\mathrm{surf}}^{-1}$. For a range of HZSM-5 materials differing only in SAR (assumed here to influence only pore surface chemistry and maintain a constant d_p) and characterised by the same probe molecule (constant D and d_k), we note that changes in this ratio will be dominated by changes in $\rho_2/\rho_1 = T_{1,\mathrm{surf}}/T_{2,\mathrm{surf}}$; this ratio is considered a probe of molecular mobility at the solid/liquid interface and is therefore sensitive to surface affinity.[32,35,39]

Experimental

Materials and sample preparation

Pyridine (≥99%) was obtained from Alfa Aesar and used as supplied. ZSM-5 zeolite powders exhibiting a range of SAR values (23, 30, 50, 80 and 300) were obtained from Alfa Aesar in NH_4^+ form. The solid powders were calcined in synthetic air (Air Liquide, 100 mL min^{-1}) at 773 K for 4 hours to obtain the protonated form, HZSM-5. We note these materials have been characterised elsewhere *via* argon sorption measurements, infrared spectroscopy, elemental analysis, solid state ^{27}Al MAS NMR spectroscopy and tapered element oscillating microbalance experiments.[70–72]

Samples for TPD and NMR analysis were first prepared by pressing each zeolite powder into tablets using a manual hydraulic press. A 2 tonne compressive force was applied to approximately 250 mg of powder in each case, forming cylindrical tables measuring around 13 mm in dimeter and 1 mm in thickness. The tablets were then broken into approximately 10 mg pieces so as to fit within the active regions of the TPD and NMR equipment. Each material was dried in N_2 (Air Liquide, 100 mL min^{-1}) at 673 K for 1 hour to remove any adsorbed water, and soaked in excess pyridine under ambient conditions for at least 24 hours.

NMR relaxation measurements

^{1}H NMR relaxation measurements were performed using a Bruker DMX 300 spectrometer equipped with a 7.1 T superconducting magnet, corresponding to a ^{1}H frequency of 300.13 MHz. Experiments were performed under ambient pressure and at 298 ± 1 K as controlled by a Bruker Variable Temperature (BVT 3000) unit.

Pyridine-saturated zeolite materials were first placed onto a pre-soaked filter paper to remove any excess liquid on the external surface, then transferred to sealed 5 mm NMR tubes. To minimise experimental uncertainties associated with the evaporation of pyridine from the zeolite structures during NMR analysis, the atmosphere within each NMR tube was saturated by placing a pyridine-soaked plug of filter paper beneath the cap. Each sample was left within the magnet bore for at least 15 minutes prior to analysis to attain thermal equilibrium.

T_1–T_2 correlation data was acquired by applying the two-dimensional (2D) NMR pulse sequence in Fig. 1, which comprises an inversion recovery component followed by a CPMG echo train.[73] The indirect (T_1) dimension was encoded using $m = 16\tau$ recovery times between 1 ms and 10 s, while data in the direct (T_2) dimension was acquired by taking the magnitude of n = 512 spin echoes separated by an echo time of t_e = 0.5 ms. Echo magnitudes $S(\tau,nt_e)$ were acquired as a single data point (white data point in Fig. 1) generating an $m \times n$ data matrix with no spectral resolution. Each experiment took approximately 30 minutes to complete and included 16 repeat scans separated by a recycle delay of $5T_1$.

The acquired 2D NMR relaxation data may be described by a Fredholm integral equation of the first kind,[74]

$$\frac{S(\tau,nt_e)}{S(\tau\to\infty,0)} = \iint K(\tau,T_1,nt_e,T_2)F(T_1,T_2)d\log(T_1)d\log(T_2) + \varepsilon(\tau,nt_e). \tag{9}$$

Here $S(\tau,nt_e)/S(\tau \to \infty,0)$ is the normalised spin echo magnitude and $\varepsilon(\tau,nt_e)$ represents the experimental noise, assumed Gaussian with zero mean. The kernel function $K(\tau,T_1,nt_e,T_2)$ describes the predicted forms of T_1 and T_2 relaxation, and for the NMR pulse sequence in Fig. 1 takes the form[75]

$$K(\tau, T_1, nt_e, T_2) = \left[1 - 2\exp\left(\frac{-\tau}{T_1}\right)\right]\exp\left(\frac{-nt_e}{T_2}\right). \tag{10}$$

Finally, $F(T_1,T_2)$ represents the desired 2D distributions of T_1 and T_2 relaxation time constants; distributions were obtained by applying a numerical inversion of the acquired 2D relaxation data according to the above expressions. As this is an ill-posed problem,[76] stability of the inverted distributions in the presence of experimental noise was achieved through the use of Tikhonov regularisation,[77] with the magnitude of the smoothing parameter chosen according to the Generalised Cross-validation method.[78] Inverted distributions were bound within the range $\{10^{-3}, 10^2\}$ s and corrected for the influence of

Open Access Article. Published on 18 June 2021. Downloaded on 10/16/2025 2:56:31 PM.
This article is licensed under a Creative Commons Attribution 3.0 Unported Licence.

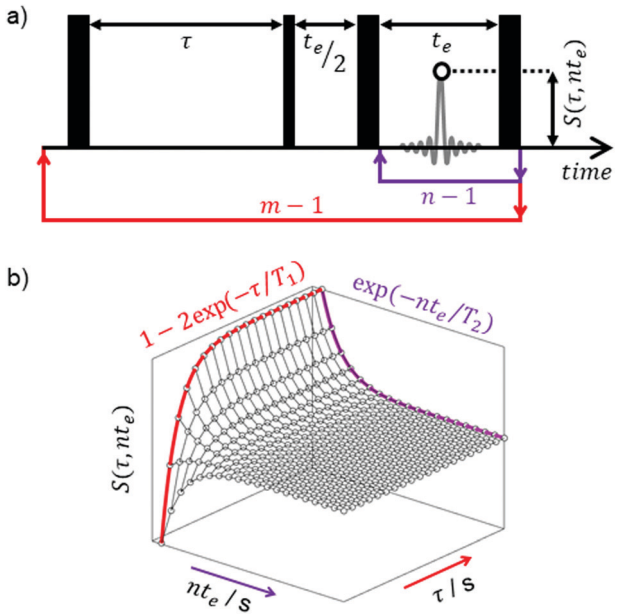

Fig. 1 (a) T_1–T_2 radio frequency (RF) pulse sequence diagram for the NMR experiments used in this work. Thick and thin solid vertical bars represent 180° and 90° RF pulses, respectively. The echo time t_e and variable recovery time τ are defined in the main text; n refocussing loops lead to n echoes separated by t_e, with the sequence is repeated to incorporate $m\times\tau$ recovery delays. An example spin echo is shown in grey, wherein the white data point indicates the echo magnitudes $S(\tau,nt_e)$ measured in this work. (b) Example 2D data surface acquired by applying the pulse sequence in (a), with the contributions of T_1 recovery and T_2 decay highlighted in the indirect and direct dimensions, respectively.

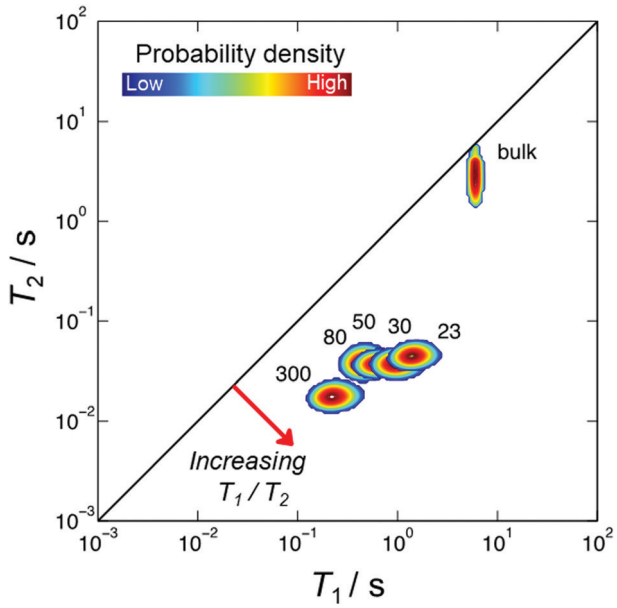

Fig. 2 ^{1}H T_1–T_2 correlation plots for pyridine in HZSM-5 with varying silica/alumina rations (SAR). Correlation peaks indicate the relative probability density of each pyridine/zeolite system exhibiting a given combination of T_1 and T_2 times, as indicated by the colour bar. The solid diagonal line indicates the parity ratio T_1/T_2 = 1. The red arrow indicates the direction of increasing T_1/T_2 ratio, which is interpreted here as indicative of surface interaction strength. SAR values are indicated next to each correlation peak; bulk pyridine data is also shown.

magnetic susceptibility contrast effects[54] using the approach of Mitchell *et al.*[79]

TPD measurements

TPD measurements were performed using a Hidden Analytical CATLAB-PCS comprising a microreactor module and integrated mass spectrometer. Zeolite samples imbibed with pyridine were placed within a glass microreactor under a constant 40 mL min^{-1} flow of high-purity helium and left for 2 hours at 432 K; after this time the mass spectrometer signal was observed to have returned to its baseline, indicating removal of all physiosorbed and excess pyridine. TPD curves were then acquired across the temperature range 423–1273 K with heating rates of β = 2, 5, 10, 15 and 20 K min^{-1}. Data from the mass fragments m/z = 52 and m/z = 79 were recorded, with each experiment repeated twice to ensure reproducibility; the acquisition of each TPD curve took between 4 and 10 hours.

Results and discussion

NMR relaxation

Fig. 2 summaries the T_1–T_2 correlation data obtained from our range of HZSM-5 zeolites. Correlation plots of this form facilitate a straightforward visual comparison of the nuclear spin relaxation characteristics exhibited by bulk (unrestricted) pyridine and pyridine adsorbed within zeolite structures of varying SAR. The diagonal line within this figure indicates T_1/T_2 = 1, characteristic of non-viscous bulk liquids.[80] The correlation peak obtained from bulk pyridine can been seen close to this diagonal, consistent with the expectation that T_1 = T_2 in the absence of surface interactions or confinement effects. Correlation peaks away from this diagonal are characterised by T_1/T_2 > 1; as suggested by eqn (8), the position of these peaks is expected to be dictated by the relative surface affinities of pyridine within these structures. The T_1/T_2 values obtained from the logarithmic mean of these correlation peaks are summarised in Table 1 and discussed further below.

Table 1 Summary of NMR and TPD results obtained from HZSM-5 zeolites with varying silica/alumina ratio (SAR). The relative errors are approximately 4% for T_1/T_2 ratio values and 3% for ΔH_{des}

SAR	T_1/T_2	ΔH_{des}/kJ mol^{-1}
23	32	150
30	25	141
50	17	132
80	14	126
300	12	110

Temperature programmed desorption

Example TPD spectra for pyridine with the range of HZSM-5 zeolites studied are shown in Fig. 3. For HZSM-5 with SAR = 23 three desorption rate maxima are evident, labelled (i), (ii) and (iii), suggesting pyridine desorbs from three distinct sites

Open Access Article. Published on 18 June 2021. Downloaded on 10/16/2025 2:56:31 PM.
This article is licensed under a Creative Commons Attribution 3.0 Unported Licence.

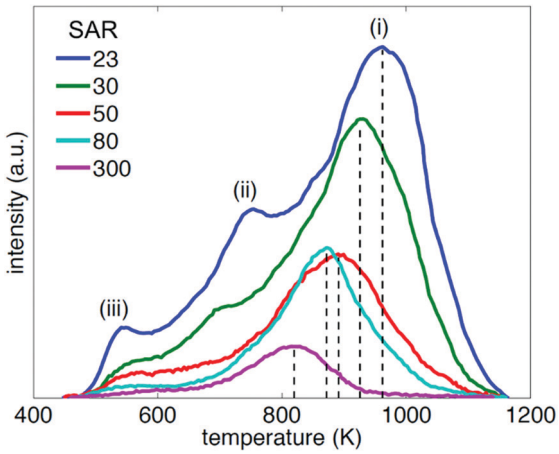

Fig. 3 Mass-normalised TPD spectra of pyridine in HZSM-5 with varying silica/alumina ratios (SAR) acquired with a heating rate of 10 K min^{-1}. Dashed lines indicate the position of the maximum desorption rate for each material.

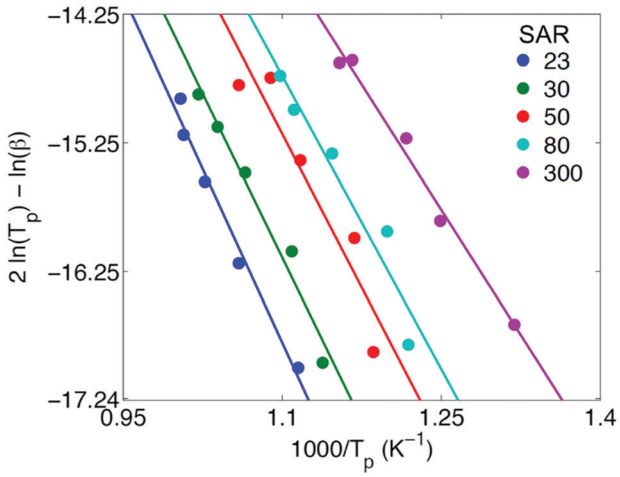

Fig. 4 TPD data acquired for pyridine desorption from HZSM-5 zeolites with varying silica/alumina ratios (SAR). Data points indicate values of the maximum desorption rate temperature T_p obtained across multiple heating rates between β = 2 K min^{-1} and β = 20 K min^{-1}. Solid lines indicate a fit to eqn (11) in each case, which yields values of the pyridine heat of desorption ΔH_{des}; the acquired values of ΔH_{des} are detailed in Table 1.

within this material. While peaks (ii) and (iii) are also evident at SAR = 30, only a single spectral desorption peak (peak (i)) is observed for the remaining materials, characterising the temperatures associated with the maximum pyridine desorption rates across these zeolites, T_p. Given the NMR relaxation time ratio T_1/T_2 is conjectured to be sensitive to the strongest adsorption sites present across a surface,[32] we focus here on the consideration of this maximum desorption rate temperature across the five materials investigated, and a comparison of the associated desorption energetics with our acquired NMR relaxation data.

Analysis of our TPD data was performed using the variable heating rate method of Cvetanović and Amenomiya,[81,82] which has been applied to a variety of acidic zeolitic systems elsewhere.[83–87] The relationship between desorption peak temperature T_p, heating rates β and the probe molecule heat of desorption ΔH_{des} may be written

$$2\ln(T_p) - \ln(\beta) = \frac{\Delta H_{\mathrm{des}}}{R}\frac{1}{T_p} + C, \qquad (11)$$

where R is the gas constant. A series of measurements utilising different heating rates therefore facilitates a plot of $2\ln(T_p) - \ln(\beta)$ against $1/T_p$, yielding a gradient equal to $\Delta H_{\mathrm{des}}/R$; this gradient is independent of the intercept parameter C, which is discussed further in the ESI.†

Fig. 4 summarises our acquired TPD data, obtained using a range of heating rates between β = 2 K min^{-1} and β = 20 K min^{-1}. Solid lines indicate a fit to eqn (11) in each case, yielding values of ΔH_{des} for each SAR. These values, together with the T_1/T_2 ratios extracted from the data within Fig. 2, are summarised in Table 1.

Correlating NMR relaxation with desorption energetics

We now provide a comparison of our acquired NMR relaxation data with the heats of desorption obtained from TPD analysis. The aim of this comparison is to validate the use of nuclear spin relaxation measurements for the comparison of zeolitic materials exhibiting different acidities, and more generally to extend the potential of such measurements – applied previously as a non-destructive probe of surface affinities in mesoporous systems – to microporous media.

The data within Table 1 reveals clear and notable correlations between SAR, T_1/T_2 ratios and ΔH_{des} values. In particular, an increase in ΔH_{des}, which correlates with decreasing SAR due to an increase in the number of Brønsted acid sites,[71] can be seen to correlate with an increase in T_1/T_2 ratio; this observation indicates the measurement of nuclear spin relaxation phenomena associated with basic probe molecules imbibed within such systems provides a useful method for the evaluation and comparison of zeolitic materials in terms of their acidity. Following our derivation of eqn (8) we attribute this observation to an increase in the ratio $T_{1,\mathrm{surf}}/T_{2,\mathrm{surf}}$ with enhanced ΔH_{des}.

In previous work an empirical theory was developed to formally relate the ratio $T_{1,\mathrm{surf}}/T_{2,\mathrm{surf}}$ with probe molecule desorption energetics.[32] It was found that a linear correlation is expected to exist between desorption energetics and the inverse relaxation time ratio $-T_2/T_1$. This relationship has been verified for a range of water[32] and short-chain hydrocarbons[39] imbibed within mesoporous catalyst support materials. To explore whether this relationship also holds within microporous structures we provide in Fig. 5 a comparison of this inverse ratio, obtained from our NMR data in Table 1 as $-T_2/T_1 = -1/(T_1/T_2)$, with our ΔH_{des} values. An extremely strong correlation is observed between these metrics, providing evidence that NMR relaxation data obtained from liquid-saturated microporous materials can provide a quantitative indication of surface interaction phenomena associated with the strongest adsorption sites present.

 This journal is © the Owner Societies 2021

Open Access Article. Published on 18 June 2021. Downloaded on 10/16/2025 2:56:31 PM.
This article is licensed under a Creative Commons Attribution 3.0 Unported Licence.

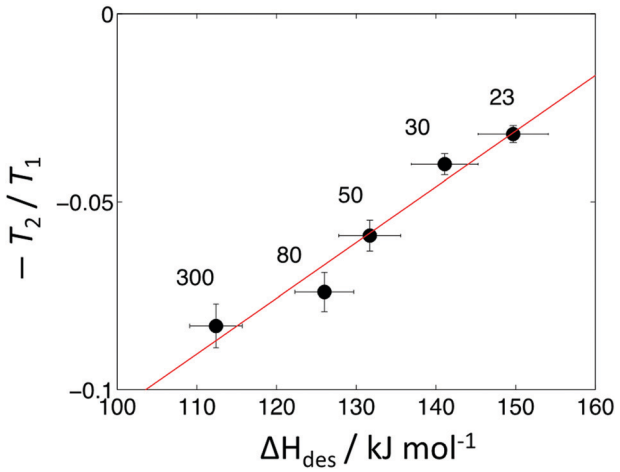

Fig. 5 Direct comparison of NMR and TPD data for pyridine adsorbed within HZSM-5 zeolites with varying silica/alumina rations (SAR). The red line is a linear fit to the data. SAR values are indicated above each data point.

Conclusions

We have detailed an investigation into the application of nuclear spin relaxation measurements as a probe of sorption energetics within microporous HZSM-5 zeolites of varying SAR. Through a direct comparison with TPD analysis our results indicate that the dimensionless ratio of relaxation time constants T_1/T_2, obtained here through the analysis of 2D ^{1}H T_1–T_2 correlation data, provides a non-invasive probe of surface affinity in microporous solids. For the specific case explored here, clear sensitivity of this relaxation time ratio to zeolite acidity has been demonstrated. Overall, our analysis method is of interest as it is rapid, non-destructive and simple to implement, and may be readily translated to portable and low-field benchtop NMR systems employed for materials screening and quality control. Measurements take on the order of tens of minutes to perform, reducing significantly the required experimental time required for such analysis compared to typical TPD analysis protocols, which may take >100 hours. Relaxation measurements may therefore be employed in standalone form to provide a rapid, qualitative indication of increasing surface interaction strength across a given material series, or performed in combination with at least two TPD calibration measurements to yield quantitative measures of surface interact strength, significantly reducing the required experimental time for such analysis. These factors suggest such relaxation time measurements represent a valuable tool for the characterisation of microporous materials.

Conflicts of interest

There are no conflicts to declare.

Acknowledgements

The authors thank Prof. Dame Lynn F. Gladden, University of Cambridge, for access to the experimental facilities. Carmine D'Agostino would also like to acknowledge the EPSRC, grant no. EP/S019138/1.

Notes and references

1 M. Shamzhy, M. Opanasenko, P. Concepción and A. Martínez, New trends in tailoring active sites in zeolite-based catalysts, *Chem. Soc. Rev.*, 2019, **48**, 1095–1149.
2 S. Mintova, M. Jaber and V. Valtchev, Nanosized microporous crystals: emerging applications, *Chem. Soc. Rev.*, 2015, **44**, 7207–7233.
3 N. Rahimi and R. Karimzadeh, Catalytic cracking of hydrocarbons over modified ZSM-5 zeolites to produce light olefins: a review, *Appl. Catal., A*, 2011, **398**, 1–17.
4 B. Xu, C. Sievers, S. B. Hong, R. Prins and J. A. van Bokhoven, Catalytic activity of Brønsted acid sites in zeolites: intrinsic activity, rate-limiting step, and influence of the local structure of the acid sites, *J. Catal.*, 2006, **244**, 163–168.
5 S. Al-Khattaf, C. D'Agostino, M. N. Akhtar, N. Al-Yassir, N. Y. Tan and L. F. Gladden, The effect of coke deposition on the activity and selectivity of the HZSM-5 zeolite during ethylbenzene alkylation reaction in the presence of ethanol, *Catal. Sci. Technol.*, 2014, **4**, 1017.
6 D. E. Bryant and W. L. Kranich, Dehydration of alcohols over zeolite catalysts, *J. Catal.*, 1967, **8**, 8–13.
7 Y. T. Kim, K.-D. Jung and E. D. Park, A comparative study for gas-phase dehydration of glycerol over H-zeolites, *Appl. Catal., A*, 2011, **393**, 275–287.
8 H. P. Decolatti, B. O. Dalla Costa and C. A. Querini, Dehydration of glycerol to acrolein using H-ZSM5 zeolite modified by alkali treatment with NaOH, *Microporous Mesoporous Mater.*, 2015, **204**, 180–189.
9 G. Busca, Acidity and basicity of zeolites: a fundamental approach, *Microporous Mesoporous Mater.*, 2017, **254**, 3–16.
10 E. G. Derouane, J. C. Védrine, R. R. Pinto, P. M. Borges, L. Costa, M. A. N. D. A. Lemos, F. Lemos and F. R. Ribeiro, The Acidity of Zeolites: Concepts, Measurements and Relation to Catalysis: A Review on Experimental and Theoretical Methods for the Study of Zeolite Acidity, *Catal. Rev.*, 2013, **55**, 454–515.
11 Y. Akacem, E. Kassab and E. Kassab, Vibrational Analysis of Pyridine Adsorption on the Brønsted Acid Sites of Zeolites Based on Density Functional Cluster Calculations, *J. Phys. Chem. C*, 2008, **112**, 19045–19054.
12 R. Buzzoni, S. Bordiga, G. Ricchiardi, C. Lamberti, A. Zecchina and G. Bellussi, Interaction of Pyridine with Acidic (H-ZSM5, H-β, H-MORD Zeolites) and Superacidic (H-Nafion Membrane) Systems: An IR Investigation, *Langmuir*, 1996, **12**, 930–940.
13 J. N. Kondo, R. Nishitani, E. Yoda, T. Yokoi, T. Tatsumi and K. Domen, A comparative IR characterization of acidic sites on HY zeolite by pyridine and CO probes with silica–alumina and γ-alumina references, *Phys. Chem. Chem. Phys.*, 2010, **12**, 11576.

Open Access Article. Published on 18 June 2021. Downloaded on 10/16/2025 2:56:31 PM.
This article is licensed under a Creative Commons Attribution 3.0 Unported Licence.

14 C. A. Emeis, Determination of Integrated Molar Extinction Coefficients for Infrared Absorption Bands of Pyridine Adsorbed on Solid Acid Catalysts, *J. Catal.*, 1993, **141**, 347–354.

15 L. Rodríguez-González, F. Hermes, M. Bertmer, E. Rodríguez-Castellón, A. Jiménez-López and U. Simon, The acid properties of H-ZSM-5 as studied by NH_3-TPD and ^{27}Al-MAS-NMR spectroscopy, *Appl. Catal., A*, 2007, **328**, 174–182.

16 F. Jin and Y. Li, A FTIR and TPD examination of the distributive properties of acid sites on ZSM-5 zeolite with pyridine as a probe molecule, *Catal. Today*, 2009, **145**, 101–107.

17 A. Camiloti, S. Jahn, N. Velasco, L. Moura and D. Cardoso, Acidity of Beta zeolite determined by TPD of ammonia and ethylbenzene disproportionation, *Appl. Catal., A*, 1999, **182**, 107–113.

18 B. Hunger, J. Hoffmann, O. Heitzsch and M. Hunger, Temperature-programmed desorption (TPD) of ammonia from HZSM-5 zeolites, *J. Therm. Anal.*, 1990, **36**, 1379–1391.

19 M. Niwa, K. Suzuki, N. Katada, T. Kanougi and T. Atoguchi, Ammonia IRMS-TPD study on the distribution of acid sites in mordenite, *J. Phys. Chem. B*, 2005, **109**, 18749–18757.

20 J. Kanellopoulos, C. Gottert, D. Schneider, B. Knorr, D. Prager, H. Ernst and D. Freude, NMR investigation of proton mobility in zeolites, *J. Catal.*, 2008, **255**, 68–78.

21 A. Zheng, S. Li and F. Deng, Solid-State NMR Characterization of Acidity of Solid Catalysts, in *Modern Magnetic Resonance*, ed. G. Webb, Springer, Cham, 2018.

22 D. Barthomeuf, Zeolite acidity dependence on structure and chemical environment. Correlations with catalysis, *Mater. Chem. Phys.*, 1987, **17**, 49–71.

23 H. M. Kao, P. C. Chang, Y. W. Liao, L. P. Lee and C. H. Chien, Solid-state NMR characterization of the acid sites in cubic mesoporous Al-MCM-48 materials using trimethylphosphine oxide as a ^{31}P NMR probe, *Microporous Mesoporous Mater.*, 2008, **114**, 352–364.

24 L. Peng, P. J. Chupas and C. P. Grey, Measuring Brønsted acid densites in zeolite HY with diphosphine molecules and solid state NMR spectroscopy, *J. Am. Chem. Soc.*, 2004, **126**, 12254–12255.

25 S. Li, S. J. Huang, W. Shen, H. Zhang, H. Fang, A. Zheng, S. Bin Liu and F. Deng, Probing the spatial proximities among acid sites in dealuminated H–Y zeolite by solid-state NMR spectroscopy, *J. Phys. Chem. C*, 2008, **112**, 14486–14494.

26 W. R. Gunther, V. K. Michaelis, R. G. Griffin and Y. Román-Leshkov, Interrogating the Lewis Acidity of Metal Sites in Beta Zeolites with ^{15} N Pyridine Adsorption Coupled with MAS NMR Spectroscopy, *J. Phys. Chem. C*, 2016, **120**, 28533–28544.

27 H. M. Kao and C. P. Grey, Probing the Brønsted and Lewis acidity of zeolite HY: A ^{1}H/^{27}Al and ^{15}N/^{27}Al TRAPDOR NMR study of monomethylamine adsorbed on HY, *J. Phys. Chem.*, 1996, **100**, 5105–5117.

28 L. F. Gladden and J. Mitchell, Measuring adsorption, diffusion and flow in chemical engineering: applications of magnetic resonance to porous media, *New J. Phys.*, 2011, **13**, 035001.

29 L. F. Gladden, Magnetic resonance in reaction engineering: beyond spectroscopy, *Curr. Opin. Chem. Eng.*, 2013, **2**, 331–337.

30 J. Kowalewski and L. Mäler, *Nuclear spin relaxation in liquids: theory, experiments, and applications*, CRC Press, 2nd edn, 2017.

31 P. A. Vecino, Z. Huang, J. Mitchell, J. McGregor, H. Daly, C. Hardacre, J. M. Thomson and L. F. Gladden, Determining adsorbate configuration on alumina surfaces with ^{13}C nuclear magnetic resonance relaxation time analysis, *Phys. Chem. Chem. Phys.*, 2015, **17**, 20830–20839.

32 C. D'Agostino, J. Mitchell, M. D. Mantle and L. F. Gladden, Interpretation of NMR Relaxation as a Tool for Characterising the Adsorption Strength of Liquids inside Porous Materials, *Chem. – Eur. J.*, 2014, **20**, 13009–13015.

33 R. Pini and L. Joss, See the unseen: applications of imaging techniques to study adsorption in microporous materials, *Curr. Opin. Chem. Eng.*, 2019, **24**, 37–44.

34 D. Weber, J. Mitchell, J. Mcgregor and L. F. Gladden, Comparing strengths of surface interactions for reactants and solvents in porous catalysts using Two-dimensional NMR relaxation correlations, *J. Phys. Chem. C*, 2009, **113**, 6610–6615.

35 J. Mitchell, L. M. Broche, T. C. Chandrasekera, D. J. Lurie and L. F. Gladden, Exploring Surface Interactions in Catalysts Using Low-Field Nuclear Magnetic Resonance, *J. Phys. Chem. C*, 2013, **117**, 17699–17706.

36 A. T. Krzyżak and I. Habina, Low field ^{1}H NMR characterization of mesoporous silica MCM-41 and SBA-15 filled with different amount of water, *Microporous Mesoporous Mater.*, 2016, **231**, 230–239.

37 K. Ralphs, C. D'Agostino, R. Burch, S. Chansai, L. F. Gladden, C. Hardacre, S. L. James, J. Mitchell and S. F. R. Taylor, Assessing the surface modifications following the mechanochemical preparation of a Ag/Al_2O_3 selective catalytic reduction catalyst, *Catal. Sci. Technol.*, 2014, **4**, 531–539.

38 D. Espinat, F. Gaulier, F. Norrant, J. Barbier, B. Guichard, M. Rivallan and P. Levitz, Characterization of Asphaltenes in Solution and Inside the Pores of Catalysts by ^{1}H NMR Relaxometry, *Energy Fuels*, 2017, **31**, 7382–7395.

39 N. Robinson, C. Robertson, L. F. Gladden, S. J. Jenkins and C. D'Agostino, Direct correlation between adsorption energetics and nuclear spin relaxation in a liquid-saturated catalyst material, *ChemPhysChem*, 2018, **19**, 2472–2479.

40 C. D'Agostino, M. R. Feaviour, G. L. Brett, J. Mitchell, A. P. E. York, G. J. Hutchings, M. D. Mantle and L. F. Gladden, Solvent inhibition in the liquid-phase catalytic oxidation of 1,4-butanediol: understanding the catalyst behaviour from NMR relaxation time measurements, *Catal. Sci. Technol.*, 2016, **6**, 7896–7901.

 This journal is © the Owner Societies 2021

Open Access Article. Published on 18 June 2021. Downloaded on 10/16/2025 2:56:31 PM.
This article is licensed under a Creative Commons Attribution 3.0 Unported Licence.

41 C. D'Agostino, R. D. Armstrong, G. J. Hutchings and L. F. Gladden, Product Inhibition in Glycerol Oxidation over Au/TiO_2 Catalysts Quantified by NMR Relaxation, *ACS Catal.*, 2018, **8**, 7334–7339.
42 J. J. Varghese, L. Cao, C. Robertson, Y. Yang, L. F. Gladden, A. A. Lapkin and S. H. Mushrif, Synergistic Contribution of the Acidic Metal Oxide-Metal Couple and Solvent Environment in the Selective Hydrogenolysis of Glycerol: A Combined Experimental and Computational Study Using ReOx–Ir as the Catalyst, *ACS Catal.*, 2019, **9**, 485–503.
43 M. Wehring, J. Gascon, D. Dubbeldam, F. Kapteijn, R. Q. Snurr and F. Stallmach, Self-diffusion studies in CuBTC by PFG NMR and MD simulations, *J. Phys. Chem. C*, 2010, **114**, 10527–10534.
44 N. Robinson, G. Xiao, P. R. J. Connolly, N. N. A. Ling, E. O. Fridjonsson, E. F. May and M. L. Johns, Low-field NMR relaxation-exchange measurements for the study of gas admission in microporous solids, *Phys. Chem. Chem. Phys.*, 2020, **22**, 13689–13697.
45 V. J. Witherspoon, R. Mercado, E. Braun, A. Mace, J. Bachman, J. R. Long, B. Blümich, B. Smit and J. A. Reimer, Combined Nuclear Magnetic Resonance and Molecular Dynamics Study of Methane Adsorption in M_2(dobdc) Metal–Organic Frameworks, *J. Phys. Chem. C*, 2019, **123**, 12286–12295.
46 F. Stallmach, A. K. Pusch, T. Splith, C. Horch and S. Merker, NMR relaxation and diffusion studies of methane and carbon dioxide in nanoporous ZIF-8 and ZSM-58, *Microporous Mesoporous Mater.*, 2015, **205**, 36–39.
47 J. J. Chen, X. Kong, K. Sumida, M. A. Manumpil, J. R. Long and J. A. Reimer, *Ex Situ* NMR relaxometry of metal–organic frameworks for rapid surface-area screening, *Angew. Chem., Int. Ed.*, 2013, **52**, 12043–12046.
48 J. J. Chen, J. A. Mason, E. D. Bloch, D. Gygi, J. R. Long and J. A. Reimer, NMR relaxation and exchange in metal–organic frameworks for surface area screening, *Microporous Mesoporous Mater.*, 2015, **205**, 65–69.
49 T. Ueda, K. Kurokawa, Y. Kawamura, K. Miyakubo and T. Eguchi, ^{1}H NMR study of molecular motion of benzene and *n*-decane confined in the nanocavities of metal–organic frameworks, *J. Phys. Chem. C*, 2012, **116**, 1012–1019.
50 V. J. Witherspoon, L. M. Yu, S. Jawahery, E. Braun, S. M. Moosavi, S. K. Schnell, B. Smit and J. A. Reimer, Translational and Rotational Motion of C8 Aromatics Adsorbed in Isotropic Porous Media (MOF-5): NMR Studies and MD Simulations, *J. Phys. Chem. C*, 2017, **121**, 15456–15462.
51 J.-P. Korb, S. Xu and J. Jonas, Confinement effects on dipolar relaxation by translational dynamics of liquids in porous silica glasses, *J. Chem. Phys.*, 1993, **98**, 2411–2422.
52 J.-P. Korb, A. Delville, S. Xu, G. Demeulenaere, P. Costa and J. Jonas, Relative role of surface interactions and topological effects in nuclear magnetic resonance of confined liquids, *J. Chem. Phys.*, 1994, **101**, 7074–7081.
53 J.-P. Korb, Nuclear magnetic relaxation of liquids in porous media, *New J. Phys.*, 2011, **13**, 035016.
54 J. Mitchell, T. C. Chandrasekera, M. L. Johns, L. F. Gladden and E. J. Fordham, Nuclear magnetic resonance relaxation and diffusion in the presence of internal gradients: the effect of magnetic field strength, *Phys. Rev. E: Stat., Nonlinear, Soft Matter Phys.*, 2010, **81**, 026101.
55 J. Mitchell and T. C. Chandrasekera, Understanding generalized inversions of nuclear magnetic resonance transverse relaxation time in porous media, *J. Chem. Phys.*, 2014, **141**, 224201.
56 Y. Q. Song, Magnetic resonance of porous media (MRPM): a perspective, *J. Magn. Reson.*, 2013, **229**, 12–24.
57 G. Liu, Y. Li and J. Jonas, Confined geometry effects on reorientational dynamics of molecular liquids in porous silica glasses, *J. Chem. Phys.*, 1991, **95**, 6892–6901.
58 R. L. Kleinberg, W. E. Kenyon and P. P. Mitra, Mechanism of NMR Relaxation of Fluids in Rock, *J. Magn. Reson., Ser. A*, 1994, **108**, 206–214.
59 S. Godefroy, J.-P. Korb, M. Fleury and R. G. Bryant, Surface nuclear magnetic relaxation and dynamics of water and oil in macroporous media, *Phys. Rev. E: Stat., Nonlinear, Soft Matter Phys.*, 2001, **64**, 021605.
60 N. Robinson, L. F. Gladden and C. D'Agostino, Exploring catalyst passivation with NMR relaxation, *Faraday Discuss.*, 2017, **204**, 439–452.
61 C. D'Agostino and P. Bräuer, Exploiting enhanced paramagnetic NMR relaxation for monitoring catalyst preparation using T_1–T_2 NMR correlation maps, *React. Chem. Eng.*, 2019, **4**, 268–272.
62 C. D'Agostino, G. Brett, G. Divitini, C. Ducati, G. J. Hutchings, M. D. Mantle and L. F. Gladden, Increased Affinity of Small Gold Particles for Glycerol Oxidation over Au/TiO_2 Probed by NMR Relaxation Methods, *ACS Catal.*, 2017, **7**, 4235–4241.
63 B. E. Kinn, T. R. Myers and A. M. Allgeier, Surface enhanced nuclear magnetic resonance relaxation mechanisms and their significance in chemical engineering applications, *Curr. Opin. Chem. Eng.*, 2019, **24**, 115–121.
64 J. P. Korb, S. Godefroy and M. Fleury, Surface nuclear magnetic relaxation and dynamics of water and oil in granular packings and rocks, *Magn. Reson. Imaging*, 2003, **21**, 193–199.
65 W. F. J. Slijkerman and J. P. Hofman, Determination of surface relaxivity from NMR diffusion measurements, *Magn. Reson. Imaging*, 1998, **16**, 541–544.
66 J. Mitchell and E. J. Fordham, Contributed Review: nuclear magnetic resonance core analysis at 0.3 T, *Rev. Sci. Instrum.*, 2014, **85**, 111502.
67 D. Ohayon, R. Le Van Mao, D. Ciaravino, H. Hazel, A. Cochennec and N. Rolland, Methods for pore size engineering in ZSM-5 zeolite, *Appl. Catal., A*, 2001, **217**, 241–251.
68 M. Che and J. C. Védrine, *Characterization of solid materials and heterogeneous catalysts: from structure to surface reactivity*, Wiley-VCH, 2012.
69 A. S. Al-Dughaither and H. De Lasa, HZSM-5 zeolites with different SiO_2/Al_2O_3 ratios. Characterization and NH3

Open Access Article. Published on 18 June 2021. Downloaded on 10/16/2025 2:56:31 PM.
This article is licensed under a Creative Commons Attribution 3.0 Unported Licence.

desorption kinetics, *Ind. Eng. Chem. Res.*, 2014, **53**, 15303–15316.

70 P. Braüer and C. D'Agostino, Base adsorption mechanism over zeolite catalysts at different Al contents probed by the tapered element oscillating microbalance (TEOM), *Phys. Chem. Chem. Phys.*, 2018, **20**, 25357–25364.

71 P. Bräuer, O. Situmorang, P. L. Ng and C. D'Agostino, Effect of Al content on the strength of terminal silanol species in ZSM-5 zeolite catalysts: a quantitative DRIFTS study without the use of molar extinction coefficients, *Phys. Chem. Chem. Phys.*, 2018, **20**, 4250–4262.

72 P. Bräuer, P. L. Ng, O. Situmorang, I. Hitchcock and C. D'Agostino, Effect of Al content on number and location of hydroxyl acid species in zeolites: a DRIFTS quantitative protocol without the need for molar extinction coefficients, *RSC Adv.*, 2017, **7**, 52604–52613.

73 Y.-Q. Song, L. Venkataramanan, M. D. Hürlimann, M. Flaum, P. Frulla and C. Straley, T_1–T_2 Correlation Spectra Obtained Using a Fast Two-Dimensional Laplace Inversion, *J. Magn. Reson.*, 2002, **154**, 261–268.

74 L. Venkataramanan, Y.-Q. Song and M. D. Hurlimann, Solving Fredholm integrals of the first kind with tensor product structure in 2 and 2.5 dimensions, *IEEE Trans. Signal Process*, 2002, **50**, 1017–1026.

75 J. Mitchell, L. F. Gladden, T. C. Chandrasekera and E. J. Fordham, Low-field permanent magnets for industrial process and quality control, *Prog. Nucl. Magn. Reson. Spectrosc.*, 2014, **76**, 1–60.

76 P. C. Hansen, Numerical tools for analysis and solution of Fredholm integral equations of the first kind, *Inverse Probl.*, 1992, **8**, 849–872.

77 A. N. Tikhonov and V. I. A. Arsenin, *Solutions of ill-posed problems*, SIAM, 1977.

78 J. Mitchell, T. C. Chandrasekera and L. F. Gladden, Numerical estimation of relaxation and diffusion distributions in two dimensions, *Prog. Nucl. Magn. Reson. Spectrosc.*, 2012, **62**, 34–50.

79 J. Mitchell, T. C. Chandrasekera and L. F. Gladden, Measurement of the true transverse nuclear magnetic resonance relaxation in the presence of field gradients, *J. Chem. Phys.*, 2013, **139**, 074205.

80 N. Bloembergen, E. M. Purcell and R. V. Pound, Relaxation effects in nuclear magnetic resonance absorption, *Phys. Rev.*, 1948, **73**, 679–712.

81 R. J. Cvetanović and Y. Amenomiya, Application of a Temperature-Programmed Desorption Technique to Catalyst Studies, *Adv. Catal.*, 1967, **17**, 103–149.

82 R. J. Cvetanoviĉ and Y. Amenomiya, A Temperature Programmed Desorption Technique for Investigation of Practical Catalysts, *Catal. Rev.*, 1972, **6**, 21–48.

83 S. B. Sharma, B. L. Meyers, D. T. Chen, J. Miller and J. A. Dumesic, Characterization of catalyst acidity by microcalorimetry and temperature-programmed desorption, *Appl. Catal., A*, 1993, **102**, 253–265.

84 N. Y. Topsøe, K. Pedersen and E. G. Derouane, Infrared and temperature-programmed desorption study of the acidic properties of ZSM-5-type zeolites, *J. Catal.*, 1981, **70**, 41–52.

85 G. I. Kapustin, T. R. Brueva, A. L. Klyachko, S. Beran and B. Wichterlova, Determination of the number and acid strength of acid sites in zeolites by ammonia adsorption. Comparison of calorimetry and temperature-programmed desorption of ammonia, *Appl. Catal.*, 1988, **42**, 239–246.

86 Y. Du, B. Wooler, M. Nines, P. Kortunov, C. S. Paur, J. Zengel, S. C. Weston and P. I. Ravikovitch, New High- and Low-Temperature Phase Changes of ZIF-7: Elucidation and Prediction of the Thermodynamics of Transitions, *J. Am. Chem. Soc.*, 2015, **137**, 13603–13611.

87 C. V. Hidalgo, H. Itoh, T. Hattori, M. Niwa and Y. Murakami, Measurement of the acidity of various zeolites by temperature-programmed desorption of ammonia, *J. Catal.*, 1984, **85**, 362–369.

 This journal is © the Owner Societies 2021